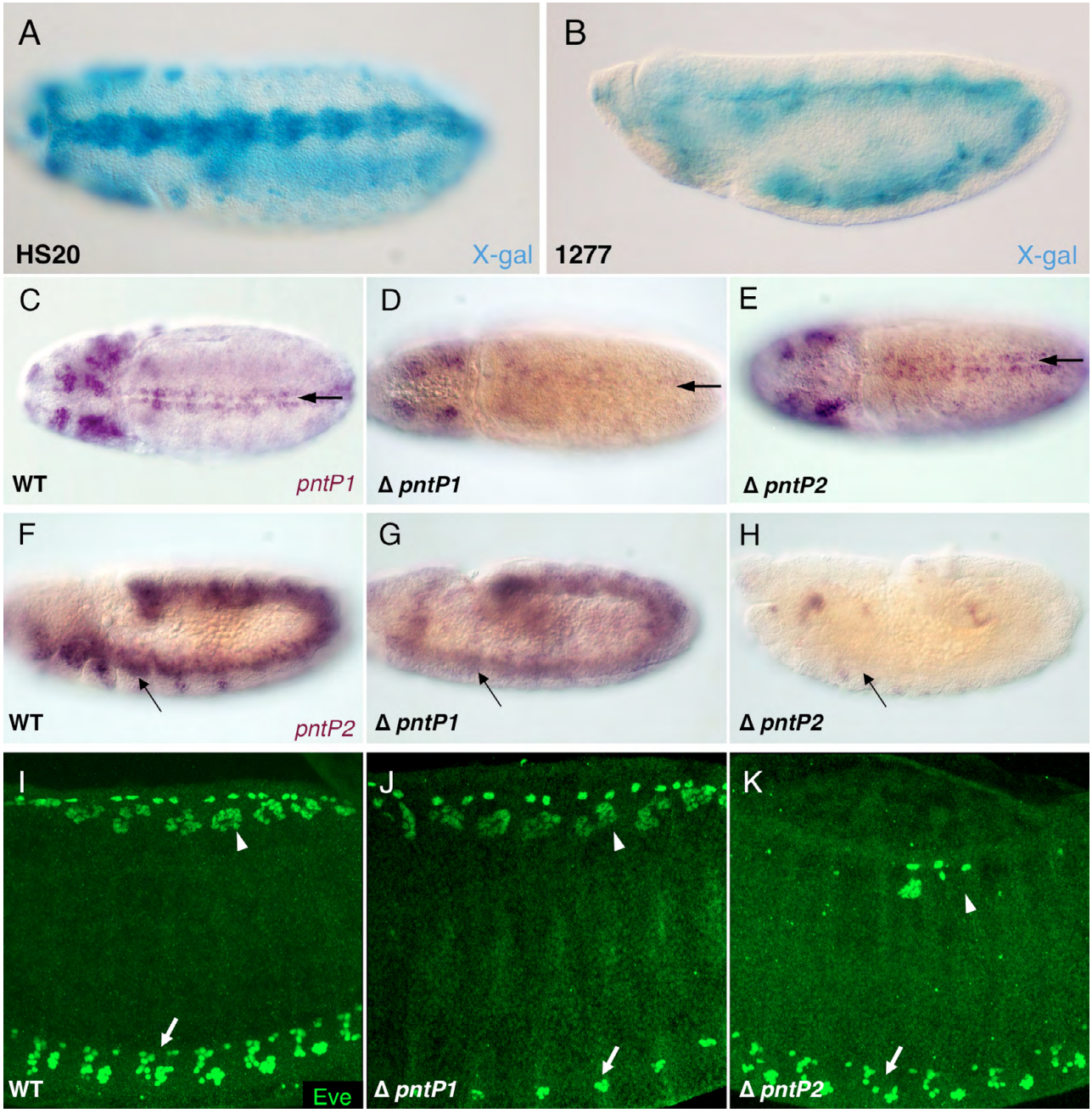

Fig. S1. HS20 and 1277 faithfully display the expression pattern of each *pnt* form, whereas $pnt^{\Delta 33}$ and $pnt^{\Delta 78}$ mutants represent specific disruptions of each of the *pnt* transcription units. (**A**,**B**) Expression pattern of the two enhancer traps in stage 10-11 embryos, monitored by X-gal staining. HS20 (*pntP1)* is detected in the ventral ectoderm (A) while 1277 (*pntP2)* is detected in the mesoderm of the embryo (B). (**C-E**) *In situ* hybridization of a *pntP1*-specific probe to stage 10-11, wild-type (C), mutant *pntP1* ($pnt^{\Delta 33}$) (D) and mutant *pntP2* ($pnt^{\Delta 78}$) (E) embryos. Arrows indicate the ventral midline. A disruption of *pntP1* expression was observed in 23% of the examined embryos (*n*=52) from a cross between $pnt^{\Delta 33}$ heterozygotes, but only in 2% of the examined embryos (*n*=86) from a cross between $pnt^{\Delta 78}$ heterozygotes. (**F-H**) *In situ* hybridization of a *pntP2*-specific probe to stage 10-11, wild-type (F), mutant *pntP1* ($pnt^{\Delta 33}$) (G) and mutant *pntP2* ($pnt^{\Delta 78}$) (H) embryos. Arrows indicate the mesoderm. Fewer than 5% of the embryos (*n*=65) from a cross between $pnt^{\Delta 33}$ heterozygotes showed abnormality in *pntP2* expression, while expression was strongly reduced or missing in 21% of the examined embryos (*n*=74), from a cross between $pnt^{\Delta 78}$ heterozygotes. (**I-K**) Anti-Eve staining of stage 14 wild-type (I), mutant *pntP1* ($pnt^{\Delta 33}$) (J) and mutant *pntP2* ($pnt^{\Delta 78}$) (K) embryos. Arrowheads indicate DA1 muscle clusters and arrows indicate the CNS. Approximately one quarter of the embryos from a cross between $pnt^{\Delta 33}$ heterozygotes (*n*=83) showed a strong reduction in Eve staining of the CNS, while the mesodermally derived DA1 clusters were unaffected (J). Conversely, DA1 cluster staining was nearly absent in approximately one quarter of the embryos from a cross between $pnt^{\Delta 78}$ heterozygotes (*n*=120). CNS staining was only weakly affected in these embryos (K).

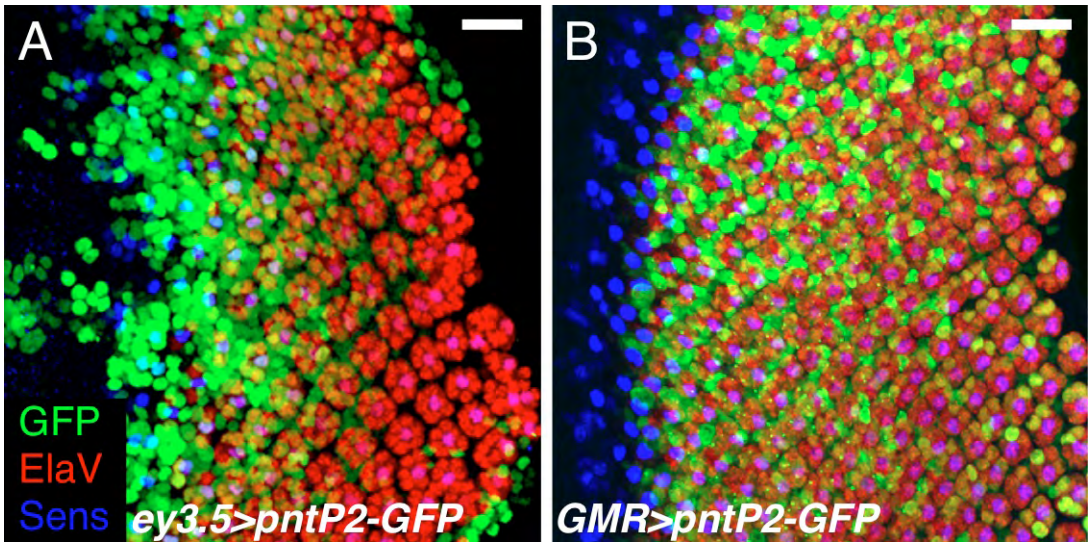

Fig. S2. The *UAS-PntP2* GFP-tagged construct is robustly expressed. (**A**,**B**) Imaginal eye discs expressing *UAS-pntP2-GFP* via the *ey3.5-Gal4* driver, which is active throughout the eye disc epithelium (A), or via *GMR-Gal4*, which is active posterior to the morphogenetic furrow (B). Photoreceptors are visualized with Elav (red) and R8 photoreceptors with Sens (blue). Visualization of PntP2-GFP using anti-GFP (green) attests to the robust levels of expression obtained using either Gal4 driver.

Table S1. Parameters used for the graph in Fig. 6A

Parameter	Physical meaning	Value
α_{Spi}	Spi production rate	10^{-3} seconds$^{-1}\mu M^{-1}$
β_{Spi}	Spi degradation rate	10^{-2} seconds^{-1}
t_0	Time when Spi values begin to drop	10^3 seconds
k_{kin}	Spi dependent PntP2 phosphorylation rate	10 seconds$^{-1}\mu M^{-1}$
τ_p	Time for the propagation of the Spi signal until PntP2 is phosphorylated	15 seconds
k_{phos}	pPntP2 dephosphorylation rate	10^{-1} seconds^{-1}
α_{P1}	pPntP2-dependent PntP1 production rate	10^{-2} seconds$^{-1}\mu M^{-1}$
τ_t	Time to produce PntP1 protein following activation by pPntP2	900 secondsa
β_{P1}	PntP1 turnover rate	1/3600 seconds^{-1}
$P2_{tot}$	Total PntP2 levels	10 μM

The time scales and lag times of phosphorylation and dephosphorylation of PntP2 are much faster than those of PntP1. This reflects the fact that signal transduction and phosphorylation are faster events than protein production and turnover rates.